Catal Lett (2012) 142:384–388
DOI 10.1007/s10562-011-0745-5

Preparation and Photocatalytic Activity of $(Cu_{0.94}La_{0.06})_2SnO_4$ Nanocomposite Photocatalyst Under Simulated Sunlight

Ling Li · Huisheng Zhuang · Dan Bu

Received: 20 February 2011 / Accepted: 16 November 2011 / Published online: 9 February 2012

Abstract A series of $(Cu_{0.94}La_{0.06})_2SnO_4$ photocatalysts were prepared under different calcination temperatures using a simple co-precipitation method. The crystalline structures of the as-prepared photocatalysts, as well as their particle sizes, photo absorption, and the effect of calcination temperature, were investigated using x-ray powder diffraction, Brunauer–Emmett–Teller method, transmission electron microscopy, and UV−Vis diffuse reflectance spectroscopy, respectively. The photocatalytic activity of $(Cu_{0.94}La_{0.06})_2SnO_4$ nanocomposite oxide was evaluated using the photodegradation efficiency of acid blue 62 (AB62) as a probe under simulated sunlight irradiation. The photocatalytic experimental results show that the maximum specific photocatalytic activity of the $(Cu_{0.94}La_{0.06})_2SnO_4$ photocatalyst appears after calcination at 450 °C for 2.5 h because of the good crystallization and small crystal size of the sample. Under simulated sunlight irradiation, the AB62 aqueous solution can reach a degradation rate of 97.71% in 2 h, showing that the $(Cu_{0.94}La_{0.06})_2SnO_4$ nanocomposite photocatalyst has a much higher photocatalytic activity than the standard Degussa P25 photocatalyst.

Keywords Photocatalysis · $(Cu_{0.94}La_{0.06})_2SnO_4$ · Calcination temperature · Simulated sunlight · Acid blue 62

L. Li · H. Zhuang (✉) · D. Bu
School of Environmental Science & Engineering, Shanghai Jiao Tong University, Shanghai 200240, People's Republic of China
e-mail: huishengzhuang@126.com; hszhuang@sjtu.edu.cn

L. Li · H. Zhuang
College of Environmental Science & Engineering, Donghua University, Shanghai 201620, People's Republic of China

1 Introduction

Semiconductor photocatalysis, one of the most efficient destructive technologies among advanced oxidation processes, has attracted extensive attention in the past 20 years. Several organic compounds have been shown to oxidize in CO_2, water, and mineral acids using semiconductor photocatalysis. Dye pollutants are the main sources of environmental contamination, and these pollutants can be effectively removed from wastewater using the photocatalytic process of semiconductor photocatalysis [1, 2]. Titanium dioxide is the most viable nanoparticle as a photocatalyst because of its optical and electronic properties, high oxidative power, stability, low cost, non-toxicity, and ability to eliminate persistent organic pollutants in water [3, 4]. However, its practical applications have been limited by its large energy band gap (E_g) of 3.2 eV [5], which can only capture less than 3% of the available solar energy ($\lambda < 387$ nm), as well as the fast recombination of its photogenerated electron–hole (e^-–h^+) pairs [6]. Therefore, developing new visible-light photocatalysts is necessary to extend the absorption wavelength range into the visible-light region [7]. A number of studies related to the photocatalytic activity of coupled semiconductor photocatalysts, including Nd_2InTaO_7 [8], $In_{1-x}M_xTaO_4$ [9], $(CuIn)_xZn_{2(1-x)}S_2$ [10], $CaTi_{1-x}Zr_xO_3$ [11], and CuO/SnO_2 [12], have recently been conducted. These semiconductor photocatalysts increase the photocatalytic efficiency by increasing the charge separation and extending the photo-responding range. In addition, these semiconductors exhibit fine optical properties compared with the corresponding bulk semiconductors because of the quantum confinement effects [13–15].

To the best of our knowledge, a $(Cu_{0.94}La_{0.06})_2SnO_4$ nanocomposite photocatalyst has not been reported. In the

current study, a series of $(Cu_{0.94}La_{0.06})_2SnO_4$ photocatalysts were prepared under different calcination temperatures (300, 450, and 600 °C) using a relatively simple co-precipitation method. Their crystalline structures, particle sizes, photo absorption, and optimum calcination temperature were investigated. The photocatalytic activities of the as-prepared catalysts were investigated by degrading dye pollutants acid blue 62 (AB62) as a model organic compound under simulated sunlight irradiation.

2 Experimental Section

2.1 Preparation of the Catalysts

In the current study, all the chemicals used were obtained from Shanghai Sinopharm Chemical Regent Company, China without further purification. The nanosized $(Cu_{0.94}La_{0.06})_2SnO_4$ photocatalysts were prepared using a simple co-precipitation method. $SnCl_4{\cdot}5H_2O$, $CuSO_4{\cdot}5H_2O$ and $La(NO_3)_3{\cdot}6H_2O$ (analytic reagent grade) were used as starting materials, and NaOH (4 mol L^{-1}) was used as the precipitator. $SnCl_4{\cdot}5H_2O$ and $CuSO_4{\cdot}5H_2O$ were mixed (the molar ratio of Cu to Sn is 2:1) and dissolved in minimum amount of deionized water. Then, $La(NO_3)_3{\cdot}6H_2O$ was added into the mixed solution and stirred at room temperature. The sodium hydroxide was added dropwise until the mixed solution completely transformed into a precipitate. The precipitate was filtered and washed with deionized water until no Cl^- was found in the filtrates. Then, the mixed solution was dispersed through ultrasonication for 30 min and aged in water at 80 °C for 10 h. After aging, the wet powder was dried in air at about 100 °C to form the precursors of the $(Cu_{0.94}La_{0.06})_2SnO_4$ photocatalysts. Finally, the precursors were calcined for 2.5 h at different calcination temperatures (300, 450, and 600 °C) in air to prepare the photocatalyst powders.

2.2 Characterization of the Catalysts

X-ray diffraction (XRD) analysis was conducted at room temperature using a Rigaku D/max-2550 PC diffractometer with Cu $K\alpha$ radiation ($\lambda = 0.15406$ nm) over the 2θ collection range of 0° to 80° to determine the crystal phase composition of the $(Cu_{0.94}La_{0.06})_2SnO_4$ photocatalyst powders. An accelerating voltage of 40 kV, emission current of 300 mA, and scanning speed of 4° min^{-1} were used. The particle morphology of the samples was measured using a Hitachi H-800 transmission electron microscope (TEM). The Brunauer–Emmett–Teller (BET) surface areas were determined using a Micromeritics ASAP 2010 nitrogen adsorption apparatus. All the samples were degassed at 180 °C prior to the BET measurements. UV–Vis diffuse reflectance spectra (UV–Vis-DRS) were recorded in air at room temperature in the wavelength range of 200 nm to 800 nm using a PELAMBDA35 spectrophotometer with an integrating sphere.

2.3 Photocatalytic Activity Measurements

The photodegradation experiments of AB62 in the aqueous solution were performed in the presence of $(Cu_{0.94}La_{0.06})_2SnO_4$ photocatalyst powders using a quartz-jacketed photoreactor under simulated sunlight irradiation. A 1,000 W Xenon lamp was used as the light source (the spectrum distribution and relative intensity of the Xenon are similar to that of sunlight). In all the experiments, the photocatalytic reaction temperature was maintained at room temperature. The AB62 was A.R. grade, and the solution concentration was 50 mg/L. The reaction suspensions were prepared by adding 0.25 g photocatalyst powders into 250 mL AB62 solutions. Prior to the photoreaction, the suspensions were stirred magnetically in the dark for 30 min to ensure an adsorption–desorption equilibrium. The Xenon light from the top irradiated the reaction mixture vertically with continuous stirring. Analytical samples were drawn from the reaction suspensions every 20 min, and the collected samples were centrifuged at 10,000 r/min for 15 min, and then filtered through a 0.2 μm Millipore filter to remove the particles. The AB62 concentrations of the filtrate were analyzed using UV–Vis spectroscopy (UV-2000) at its maximum absorption wavelength of 595 nm.

3 Results and Discussion

3.1 Catalyst Characterization

XRD analysis was used to investigate the phase structure of the samples. Figure 1 shows the XRD patterns of the $(Cu_{0.94}La_{0.06})_2SnO_4$ nanocomposite photocatalysts calcined at 300, 450, and 600 °C for 2.5 h, respectively. The diffraction pattern of the sample prepared at 300 °C was indistinct due to the amorphous configuration or the high dispersion. The diffraction peaks of the sample prepared at 450 °C increased and can be indexed with the SnO_2, CuO, and La_2O_3 phases. When the calcination temperature reached 600 °C, no other new peaks were detected, and the width of the peak became gradually narrower due to the growth of crystallites or enhancement of crystallization. The XRD analysis of the samples showed that the CuO, La_2O_3, and SnO_2 in the $(Cu_{0.94}La_{0.06})_2$ nanocomposite photocatalyst exist in the form of a physical mixture, not a core/shell type.

The BET surface area and the average crystallite size of the $(Cu_{0.94}La_{0.06})_2SnO_4$ photocatalysts are given in

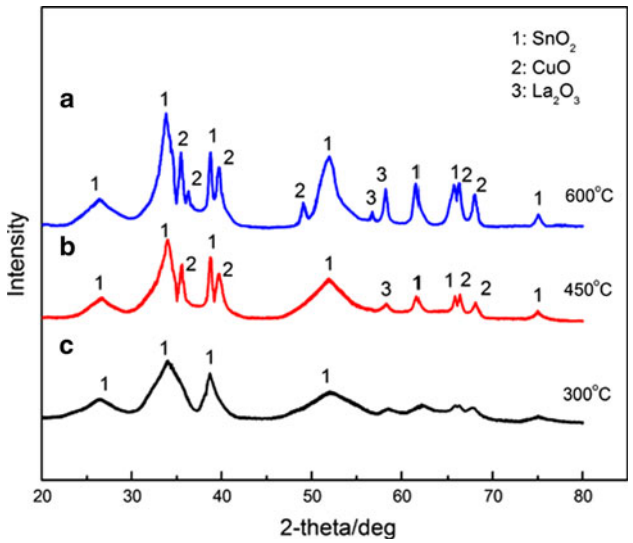

Fig. 1 XRD patterns of the $(Cu_{0.94}La_{0.06})_2SnO_4$ nanocomposite photocatalysts calcined at (*a*) 300 °C, (*b*) 450 °C, and (*c*) 600 °C for 2.5 h

Table 1 Effect of calcination temperature on the average crystallite size and surface area of the $(Cu_{0.94}La_{0.06})_2SnO_4$ photocatalysts

Calcination temperature (°C)	300	450	600
BET surface area (m^2/g)	45.76	20.35	7.91
Crystallite size (nm)	8.5	15.4	38.6

Table 1. The surface areas of the samples change considerably depending on the calcination temperature. The average crystallite size of the samples increases and the surface areas decrease with increasing calcination temperature [16].

The morphology of the samples was detected using TEM. Figure 2 shows the TEM images of the $(Cu_{0.94}La_{0.06})_2SnO_4$ nanocomposite photocatalysts prepared under different calcination temperatures. The sample calcined at 300 °C appeared amorphous because of its weak crystallization, and the grain edges were a little dim. The sample calcined at 450 °C showed homogenous and relatively small grain sizes. The sample calcined at 600 °C displayed greater particle sizes and more aggregated crystalline grains. Thus, the increase in calcination temperature may cause larger $(Cu_{0.94}La_{0.06})_2SnO_4$ photocatalyst particles. Therefore, determining the optimal temperature at which the photocatalyst shows the highest photocatalytic activity is necessary.

Figure 3 shows the UV–Vis-DRS of the as-prepared $(Cu_{0.94}La_{0.06})_2SnO_4$ photocatalysts calcined at 300, 450, and 600 °C. The absorption measurements of the samples at higher temperature show more drastic and stronger photoabsorption in the range of 400 nm to 800 nm compared with those at lower temperature. The sample calcined at 300 °C had little absorption in the range of visible-light. With the increase in calcination temperature, the absorption edge of the sample exhibited some red shifts at

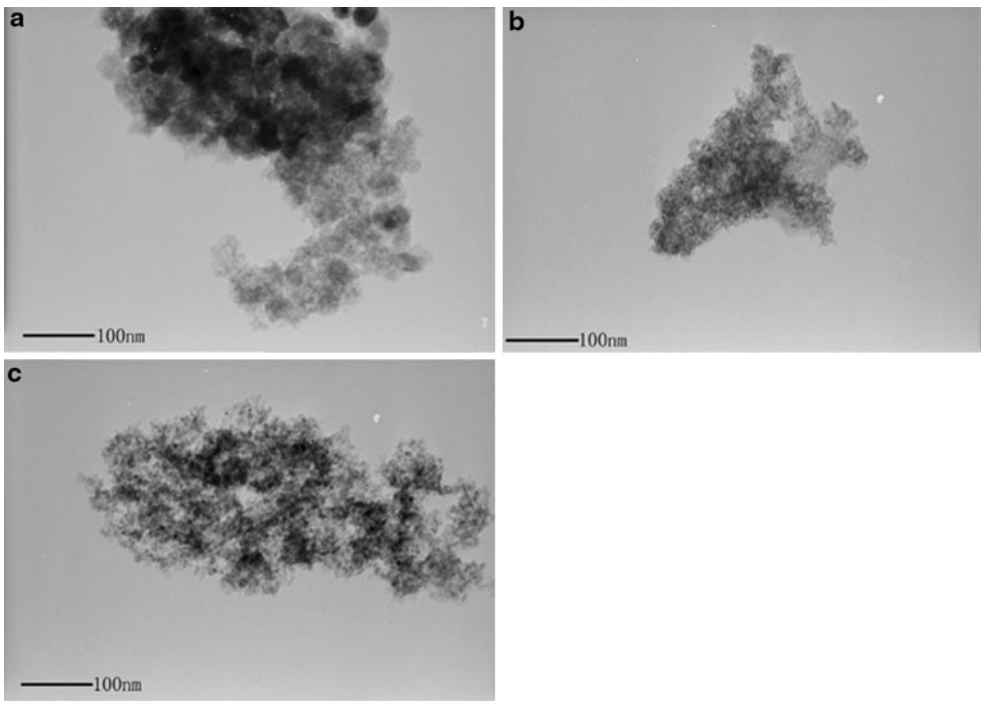

Fig. 2 TEM images of the $(Cu_{0.94}La_{0.06})_2SnO_4$ nanocomposite photocatalysts calcined at (*a*) 300 °C, (*b*) 450 °C, and (*c*) 600 °C for 2.5 h

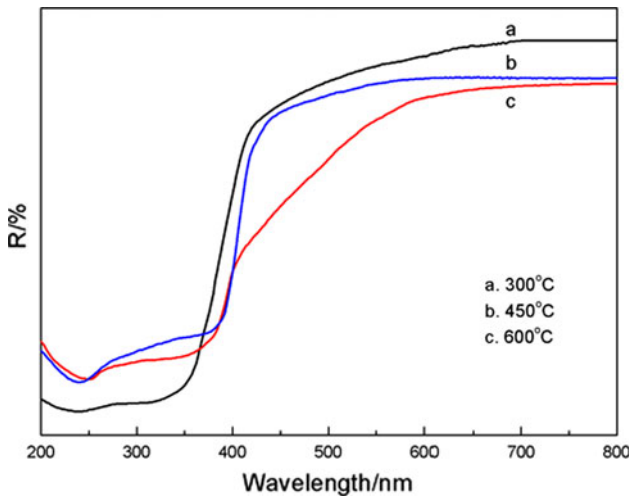

Fig. 3 UV–Vis-DRS of the $(Cu_{0.94}La_{0.06})_2SnO_4$ nanocomposite photocatalysts calcined at (*a*) 300 °C, (*b*) 450 °C, and (*c*) 600 °C for 2.5 h

450 °C, and then showed redder shifts when the calcination temperature reached 600 °C. The shifts can be ascribed to the synergetic effects of enlarged crystallite size and better crystallization, confirmed using the XRD and TEM characterizations. The E_g values for the different samples were calculated using the equation $\alpha\ (h\nu) = A\ (h\nu - E_g)^{m/2}$, where α is the absorption coefficient, $h\nu$ is the photon energy, A is a proportional constant, and $m = 1$, which represents a directly allowed transition between the valence and the conduction bands. In the estimation of E_g from the UV–Vis spectra, a straight line was extrapolated from the absorption curve to the abscissa axis [17]. The $(Cu_{0.94}La_{0.06})_2SnO_4$ photocatalyst powders prepared under different calcination temperatures of 300, 450, and 600 °C had E_g values of 2.28, 1.69, and 1.34 eV, respectively. These findings show that the E_g values decrease with increasing calcination temperature. In all cases, the E_g values of the $(Cu_{0.94}La_{0.06})_2SnO_4$ were lower than those in the TiO_2 P25 reference catalyst (3.0 eV).

3.2 Photocatalytic Activity Studies

Calcination temperature has a significant effect on the activity and stability of catalysts. Figure 4 shows the dependence of photocatalytic activity on the calcination temperature under simulated sunlight, including the evolution of AB62 in the dark (30 min) and the adsorption. The $(Cu_{0.94}La_{0.06})_2SnO_4$ nanocomposite photocatalyst calcined at 450 °C for 2.5 h reached the highest photocatalytic activity in 120 min, with the AB62 solution almost completely decolorized, which can be attributed to the sample with good crystallization and small crystal sizes. However, the photocatalytic activity of the photocatalyst decreased when the calcination temperature decreased from 450 to 200 °C because of the weak crystallization of the photocatalyst prepared under lower temperatures. In addition, the photocatalytic activity of the photocatalyst also decreased when the calcination temperature increased from 450 to 700 °C because of some sintering, although it had better crystallization.

The photocatalytic activity of the standard Degussa P25 TiO_2 was used as a reference to explore the photocatalytic activity in the degradation of AB62 under simulated sunlight irradiation of the $(Cu_{0.94}La_{0.06})_2SnO_4$ nanocomposite photocatalyst calcined at 450 °C for 2.5 h. The results are presented in Fig. 5. Under simulated sunlight irradiation, the $(Cu_{0.94}La_{0.06})_2SnO_4$ photocatalyst displays good degradation ability for AB62 of up to 97.71% in 2 h, which is obviously higher than the value of 57.81% of Degussa P25

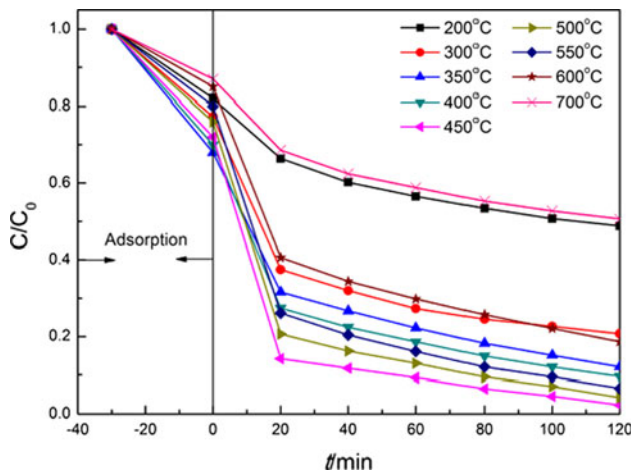

Fig. 4 Photocatalytic activities of the $(Cu_{0.94}La_{0.06})_2SnO_4$ photocatalysts calcined at different temperatures for AB62 under simulated sunlight irradiation for 2 h

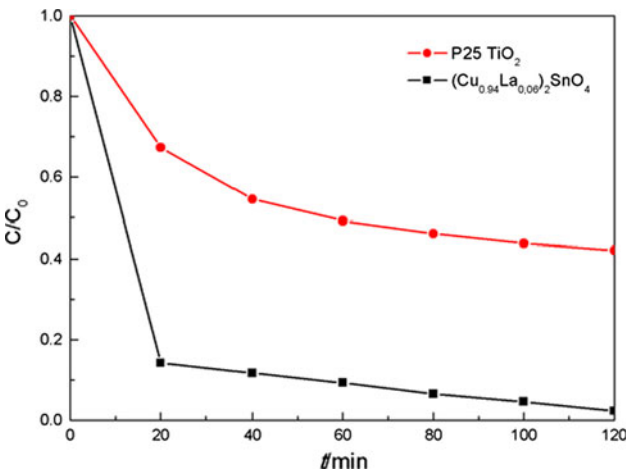

Fig. 5 Comparisons of the photocatalytic activities of the $(Cu_{0.94}La_{0.06})_2SnO_4$ photocatalyst with P25 for the degradation of AB62 under simulated sunlight irradiation for 2 h

under the same conditions. The enhanced photocatalysis may be due to the synergetic effect on the specific adsorption property and efficient electron–hole separation at the $(Cu_{0.94}La_{0.06})_2SnO_4$ nanocomposite photocatalyst interfaces.

4 Conclusion

A series of nanosized $(Cu_{0.94}La_{0.06})_2SnO_4$ photocatalysts prepared under different calcination temperatures were synthesized using a simple co-precipitation method. The characterizations of XRD, BET, TEM, and UV–Vis-DRS showed that the sample calcined at 450 °C for 2.5 h has good crystallization, smaller crystal sizes, and stronger response to simulated sunlight compared with the samples calcined at other temperatures. The $(Cu_{0.94}La_{0.06})_2SnO_4$ photocatalyst showed a more remarkable photocatalytic activity compared with that of the standard P25 photocatalyst, and 97.71% AB62 can be degraded in 2 h under simulated sunlight irradiation. The manner by which high photocatalytic activity is maintained after recycling the $(Cu_{0.94}La_{0.06})_2SnO_4$ photocatalyst is currently under investigation. The effective photodegradation dye using the $(Cu_{0.94}La_{0.06})_2SnO_4$ photocatalyst under simulated sunlight is a very exciting application in the photocatalytic area, and the current study may provide new insights into the development of novel sunlight photocatalysts.

Acknowledgments The authors gratefully acknowledge the financial supports from the Key Scientific and Technological Project of Shanghai (No. 09231202805), and the Shanghai Leading Academic Discipline Project (No. B604).

References

1. Su YY, Deng LP, Zhang N, Wang XT, Zhu XB (2009) Catal Lett 98:227
2. Garza-Tovar LL, Torres-Martínez LM, Rodríguez DB, Gómez R, Angel G (2006) J Mol Catal A 247:283
3. Kuwahara Y, Kamegawa T, Mori K, Yamashita H (2010) Curr Org Chem 14:616
4. Zheng S, Cai Y, O'Shea KE (2010) J Photochem Photobiol A 210:61
5. Khan U, Benabderrazik N, Bourdelais AJ, Baden DG, Rein K, Gardinali PR, Arroyo L, O'Shea KE (2010) Toxicon 55:1008
6. Tao Y, Xin T, Lin Z, Yu XY, Peng C, Jing W (2010) Chem Eng J 157:86
7. Khan R, Kim TJ (2009) J Hazard Mater 163:1179
8. Tang XD, Ye HQ, Zhao Z, Liu H, Ma CX (2009) Catal Lett 133:362
9. Ye JH, Zou ZG (2005) J Phys Chem Solids 66:266
10. Zhang XH, Du YC, Zhou ZH, Guo LJ (2010) Int J Hydrogen Energy 35:3313
11. Sun W, Zhang SQ, Wang C, Liu ZX, Mao ZQ (2007) Catal Lett 119:148
12. Xia HL, Zhuang HS, Zhang T, Xiao DC (2007) J Environ Sci 19:1141
13. Luan JF, Zou ZG, Lu MH, Chen YF (2009) Mater Chem Phys 98:434
14. Jing LQ, Qu YC, Wang BQ, Li SD, Jiang BJ, Yang LB, Fu W, Fu HG, Sun JZ (2006) Sol Energy Mater Sol Cells 90:1773
15. Du YL, Zhang N, Wang CM (2010) Catal Commun 11:670
16. Neppolian B, Kim Y, Ashokkumar M, Yamashita H, Choi H (2010) J Hazard Mater 182:557
17. Garza-Tovar LL, Torres-Martínez LM, Rodríguez DB, Gómez R, Angel G (2006) J Mol Catal A 247:283